Characterising the temporal evolution of fixation in human post mortem brain via linear relaxometry modelling – a marker of cross-linking?

Siawoosh Mohammadi[1,2], Sebastian Papazoglou[1], Herbert Mushumba[3], Mohammad Ashtarayeh[1], Klaus Püschel[3], Gunther Helms[4], Martina F Callaghan[5], Nikolaus Weiskopf[2], and Tobias Streubel[1,2]

[1]Department of Systems Neuroscience, Medical Center Hamburg-Eppendorf, Hamburg, Germany, [2]Department of Neurophysics, Max Planck Institute for Human Cognitive and Brain Sciences, Leipzig, Germany, [3]Department of Legal Medicine, Medical Center Hamburg-Eppendorf, Hamburg, Germany, [4]Department of Clinical Sciences Lund, Lund University, Lund, Sweden, [5]Wellcome Centre for Human Neuroimaging, UCL Institute of Neurology, London, United Kingdom

Synopsis

MRI-based biophysical models are typically validated by comparison to ex-vivo histology of fixed tissue. The fixation process itself and the accompanied autolysis processes strongly modify tissue composition, and lead to MR signal changes, making the validation of biophysical models for in vivo MRI particularly challenging. To better understand the temporal evolution of the fixation process within the whole brain and its influence on MRI parameters, we monitor the temporal evolution of the fixation process of a whole human post-mortem brain using the linear relaxometry model across 15 time-points comprised of one unfixed, in-situ MRI scan and 14 ex-vivo MRI scans at different stages of the fixation process (days 1-93).

Introduction

MRI-based biophysical models are typically validated by comparison to ex-vivo histology [1]. For most histological analyses of human brain samples, the tissue has to be fixed using immersion fixation in a paraformaldehyde (PFA) solution [2]. The fixation process in small tissue samples is known to happen in two stages: an initial, reversible stage of cross-linking that occurs rapidly (within days), and a second stage where stable, covalent cross-linking are formed (months) [2]. The fixation process itself, and the accompanied autolysis processes, strongly modify tissue composition, causing MR signal changes. In this study, we monitored the fixation process by acquiring the quantitative multi-parameter mapping (MPM) protocol before starting the fixation process (in-situ MRI) as well as during fixation (ex-vivo MRI). We additionally made use of the fast-exchange empirical relation (Fig. 1) between the longitudinal relaxation rate R_1 and the magnetization saturation rate MT and effective transverse relaxation rate R_2^*, which is described by the linear relaxometry model [3].

Methods

Sample: One human postmortem brain was obtained at autopsy with prior informed consent (WF-74/16, 37yo, female, cardiac failure, postmortem time: 21h), following a typical protocol for ex-vivo histology [2], including fixation in 4% PFA.

MRI: Measurements were performed on a 3T PRISMA fit MRI (Siemens Healthcare, Erlangen, Germany) using MPM4 protocol, comprised of calibration [5] and spoiled multi-echo fast-low-angle-shot (FLASH) [6] data with three different weightings. The parameters were: whole brain acquisitions, isotropic resolution of 1mm³, 6° (MT- and PD-weighted) and 21° (T1-weighted) flip angles, 16 gradient echoes (2.34-41.44 ms, in steps of 2.30 ms), readout bandwidth of 488 Hz/pixel, repetition time (TR): 47.50 ms. Quantitative R_2^*, R_1, and MT maps were calculated using the MPM framework[4]. The protocol was used to scan the brain first in-situ (day 0), i.e. in unfixed and still inside the skull, and ex-vivo in the 4% PFA solution at 14 time-points during the fixation process. A custom-made sample holder was used to stabilize the positioning.

Preprocessing and analysis: The MPM maps across time-points were aligned to each other using manual and non-linear, longitudinal registration available in SPM. Then, the linear relaxometry model [3] as described in Fig. 1 was used. Finally, fiber-tract region-of-interests (ROIs) as defined in the Jülich-white-matter atlas [8,9] were registered to the longitudinally registered MPM map.

Results

The relaxation parameters of the in-situ measurement (day 0) were slightly different than the in-vivo parameters from literature [3] (Fig. 1), which could be explained by differences in tissue temperature [10] or alternatively by the difference in the MPM protocol parameters (e.g. different TRs or number of echoes). All relaxometry parameters varied during the fixation (Fig. 2): while β_0 was already increased at the first measurement point after fixation (day 3) and almost stayed constant afterward, β_1 dropped first, but then increased monotonically, β_2 behaved similarly to β_1. The spatial pattern of the model residuals strongly varied across the fixation time (Fig. 3 and Fig. 5). Moreover, the change of the model residuals across time could be divided into two stages in all investigated fiber pathways: before and after day 14 (Fig. 4b). A region corresponding to the superior-longitudinal fasciculus (slf) showed particularly large residuals until day 14 (red box in Fig. 3, purple line in Fig. 4b, arrows in Fig. 5). The large residuals were caused by very small R_1 values that were not captured by the corresponding surrogate markers for myelin and iron, i.e. MT, and R_2^* (Fig. 3), indicating that the slf is differently affected by the fixation process than other fibers.

Discussion and Conclusion

Using the linear relaxometry model to monitor the fixation process, we found that: (a) each model coefficient had a distinct temporal dependence, and (b) the model residuals underwent rapid change in the first two weeks in the investigated fiber pathways. We hypothesize that these observations capture the aspects of the fixation process: the early changing β_0 captures reversible cross-linking, the permanently changing β_1 and β_2 capture the permanent covalent cross-linking, and the model residuals capture both stages as well as their spatial pattern. The observation of larger model residuals in the slf than in other fiber pathways might also reflect differences in underlying microstructure, which is captured only by R_1 due to its additional sensitivity to the microgeometry of axons[11]. More detailed data collection and analyses are planned to further test our hypothesis and interpretation: we will (i) increase temporal sampling, (ii) make additional measurements in PBS to wash out the remaining reversible cross-links, (iii) and increase our sample-size.

Acknowledgements

This work was supported by the German Research Foundation (DFG Priority Program 2041 "Computational Connectomics", [AL 1156/2-1;GE 2967/1-1; MO 2397/5-1; MO 2249/3–1], by the Emmy Noether Stipend: MO 2397/4-1) and by the BMBF (01EW1711A and B) in the framework of ERA-NET NEURON. The research leading to these results has received funding from the European Research Council under the European Union's Seventh Framework Programme (FP7/2007-2013) / ERC grant agreement n° 616905.

References

1. Weiskopf, N., Mohammadi, S., Lutti, A. & Callaghan, M. F. Advances in MRI-based computational neuroanatomy: from morphometry to in-vivo histology. Current Opinion in Neurology 28, 313–322 (2015).

2. Thavarajah, R., Mudimbaimannar, V. K., Elizabeth, J., Rao, U. K. & Ranganathan, K. Chemical and physical basics of routine formaldehyde fixation. J Oral Maxillofac Pathol 16, 400–405 (2012).

3. Callaghan, M. F., Helms, G., Lutti, A., Mohammadi, S. & Weiskopf, N. A general linear relaxometry model of R1 using imaging data. Magn Reson Med 73, 1309–1314 (2015).

4. Weiskopf, N. et al. Quantitative multi-parameter mapping of R1, PD*, MT and R2* at 3T: a multi-center validation. Front. Neurosci. 7:, 95 (2013).

5. Lutti, A. et al. Robust and fast whole brain mapping of the RF transmit field B1 at 7T. PLoS ONE 7, e32379 (2012).

6. Frahm, J., Haase, A. & Matthaei, D. Rapid three-dimensional MR imaging using the FLASH technique. J Comput Assist Tomogr 10, 363–368 (1986).

7. Ashburner, J. A fast diffeomorphic image registration algorithm. NeuroImage 38, 95–113 (2007).

8. Bürgel, U. et al. White matter fiber tracts of the human brain: Three-dimensional mapping at microscopic resolution, topography and intersubject variability. NeuroImage 29, 1092–1105 (2006).

9. Eickhoff, S. B. et al. A new SPM toolbox for combining probabilistic cytoarchitectonic maps and functional imaging data. NeuroImage 25, 1325–1335 (2005).

10. Birkl, C. et al. Effects of formalin fixation and temperature on MR relaxation times in the human brain. NMR Biomed 29, 458–465 (2016).

11. Harkins, K. D., et al., The microstructural correlates of T1 in white matter. Magn. Reson. Med., 75: 1341-1345 (2016).

Figures

$$\overrightarrow{R_1} = \left(\vec{1} \quad \overrightarrow{MT} \quad \overrightarrow{R_2^*}\right)\begin{pmatrix}\beta_0\\ \beta_1\\ \beta_2\end{pmatrix} + \vec{\epsilon}$$

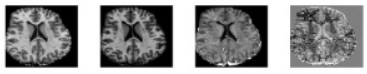

$$\vec{\varepsilon} \equiv \frac{\vec{\epsilon}}{\langle\overrightarrow{R_1}\rangle}$$

The linear relaxometry model[3] describes an empiric relation between the longitudinal relaxation rate R_1 and the magnetization saturation rate MT and apparent transverse relaxation rate R_2^*, with MT and R_2^* being surrogate markers for macromolecular and iron concentrations, respectively. The model parameters being global constants, with β_0 being the relaxation of free water, and ϵ are the spatially specific model residuals (ε is ϵ normalized by the mean of the data), encompassing noise and other unspecified contributions to R_1 that could not be captured by MT and R_2^*. The model is solved for a set of voxels in the brain.

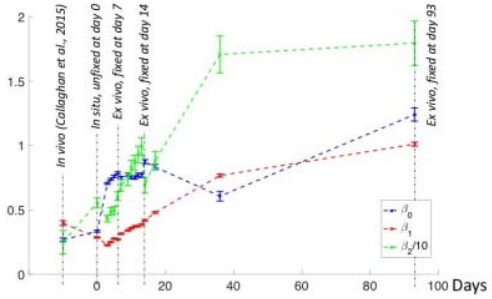

The parameters of the model in Fig. 1 were estimated from MPM parameters R_1, MT and R_2^* measured at 15 time point, consisting of 14 ex-vivo MRIs in the PFA fixative (days: 1,3,4,5,6,7,9,10,11,12,13,14,17,36,93) and one in-situ MRI (day 0). The corresponding maps of representative days (dashed lines) are presented in Fig. 3. For comparison, literature in-vivo beta values[3] are depicted as well. For the in-situ and ex-vivo measurements, the error bars are the standard-error of the mean across 1000 repetitions of estimating the betas from 300 random voxels. Dimensions of betas: $\beta_0 \quad [s^{-1}]$, $\beta_1 \quad [\frac{s^{-1}}{p.u.}]$, $\beta_2 \quad [p.u.]$.

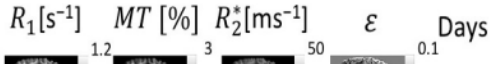

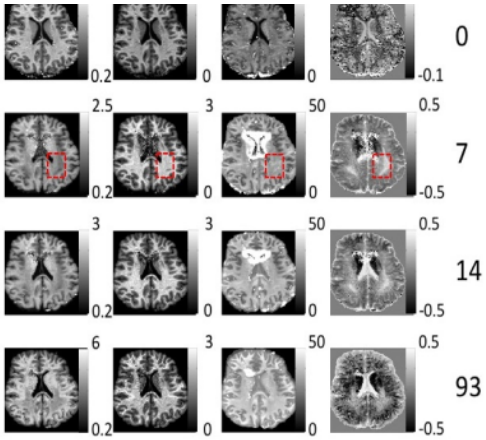

MPM parameters maps R_1, MT and R_2^* measured at time points 0, 7, 14, and 93 (see Fig. 2), as well as the normalized model residual map ε. A region, which corresponds to the superior-longitudinal fasciculus (red dashed square in 2nd row), features small R_1 values and large residuals (days 7, 14) as compared to the surrounding white matter. Note that for the R_1, and ε maps, the scaling changes across time points. The bright regions in the R_2^* maps are due to air bubbles and were masked out for all analyses.

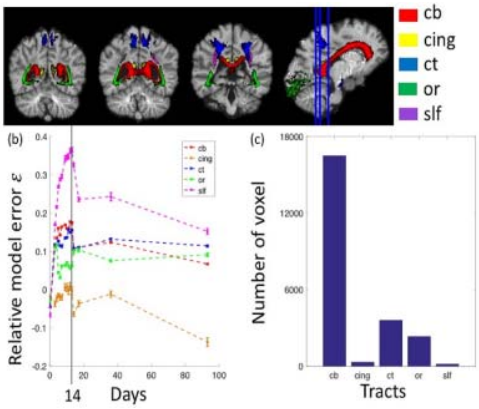

Depicted are the mean, normalized model residuals ε and its standard error of the mean (b) for 15 different time points (days:0-93, see Fig. 2 for more details) within five different fiber tracts (a). The slf shows the highest residual error, particularly until day 14. The number of voxels covered by the tracts is depicted in (c) – all tracts cover more than 100 voxels, with cb covering the most voxels. To identify the tracts the Jülich-white-matter atlas in SPM was used [8,9]. Abbreviations: cb: callosal body; cing: cingulum; ct: cortico-spinal tracts; or: optic radiation; slf: superior-longitudinal fasciculus.

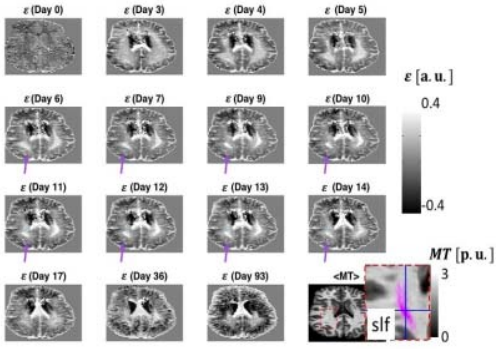

Maps of the normalized model residuals ε at different stages of the fixation process (day: 1-93) and before fixation (day 0). In addition, the MT map, averaged across all time points (<MT>), is depicted for anatomical orientation, including the magnification of a white-matter region containing the slf (overlaid in purple, see Fig. 4 for details). At day 3, a spatially circular pattern of increased ε is visible, probably indicating the penetration rim of the fixative. Between days 6-14, the shape of increased ε matches the known fiber architecture of the superior-longitudinal fasciculus (slf, arrows).